Inorganic Chemistry Communications 137 (2022) 109174

Contents lists available at ScienceDirect

Inorganic Chemistry Communications

journal homepage: www.elsevier.com/locate/inoche

Short communication

# $Ca_{12}O_{12}$ nanocluster as highly sensitive material for the detection of hazardous mustard gas: Density-functional theory

Rudi Kartika [a], Forat H. Alsultany [b], Abduladheem Turki Jalil [c,d,e], Mustafa Z. Mahmoud [f,g], Mohammed N. Fenjan [h], Halimeh Rajabzadeh [i,*]

[a] Study Program of Chemistry, Universitas Mulawarman, Samarinda 75119, Indonesia
[b] Medical Physics Department, Al-Mustaqbal University College, Hillah, Babil 51001, Iraq
[c] Faculty of Biology and Ecology, Yanka Kupala State University of Grodno, Grodno 230023, Belarus
[d] College of Technical Engineering, The Islamic University, Najaf, Iraq
[e] Department of Dentistry, Kut University College, Kut, Wasit 52001, Iraq
[f] Department of Radiology and Medical Imaging, College of Applied Medical Sciences, Prince Sattam bin Abdulaziz University, Al-Kharj 11942, Saudi Arabia
[g] Faculty of Health, University of Canberra, Canberra, ACT, Australia
[h] College of Health and Medical Technology, Al-Ayen University, Thi-Qar, Iraq
[i] Department of Chemistry, Dezful Branch, Islamic Azad University, Dezful, Iran

ARTICLE INFO

*Keywords:*
Mustard gas
Binding energies
Recovery time
Electronic characteristics
Frontier molecular orbitals

ABSTRACT

Through density functional theory (DFT) computations, the adsorption behavior and electronic sensitivity of the mustard gas are scrutinized towards a $Ca_{12}O_{12}$ nanocluster. To further investigate the influence of the molecules mentioned above over the chemical and electronic characteristics of this nanocluster, we calculate the binding energies (BEs), natural bond orbital (NBO) charge transport, the frontier molecular orbitals (FMOs), as well as molecular electrostatic potential (MEP). The interaction of the mustard molecule with the Ca atoms of the cluster through the Cl-side is slightly strong, and there is a large transport of charge from the mustard to the nanocluster. Following the adsorption of the mustard gas, there is a 2.28 eV reduction in the energy gap of the HOMO as well as the LUMO of this nanocluster. This shows that the dissociation process increases the electrical conductivity of this nanocluster to a great extent. The electrical signal which is generated is conducive to the detection of the mustard molecule. Moreover, this nanocluster has a short recovery time as a sensor. In addition, the electronic characteristics and the geometry parameters of the mustard/ $Ca_{12}O_{12}$ nanocluster complexes are impacted by the solvent to a great extent. Finally, in comparison with the vacuum, the interaction among components is significantly weaker in the aqueous phase.

## 1. Introduction

After the fullerene discovery ($C_{60}$) by Kroto et al. in 1985 [1], the field witnessed a great deal of studies into obtaining novel types of materials which were spherical in morphology, known as nanoclusters or nanocages. $(XY)_n$ is one of the most intriguing nanoclusters and its most stable state is when n = 12 [2–8]. Although no clear explanation exists regarding these wonderful arrangements, it satisfies the tetragonal rule. The $(XY)_{12}$ nanocluster is a truncated octahedron with 8 hexagons and 6 squares. $B_{12}N_{12}$ is one of $(XY)_{12}$ nanoclusters which has been characterized most. High-resolution transmission electron microscopy (HRTEM) images were used for observing $B_{12}N_{12}$ [9–12] and later the mass spectrums were used for its characterization [13–18]. The application of this nanocluster was scrutinized at the theoretical level to detect various gases such as NO [19], $NO_2$ [20], and $CO_2$ [21]; to remove arsenite and arsenate [22]; and to store hydrogen [23]. Zinc oxide (ZnO) is another nanocluster with outstanding catalytic, optical and piezoelectric properties which is also used in gas sensors as a semiconductor. Nanoparticles, nanowires, and nanotubes are among other synthesized ZnO structures which have been reported in the literature [24]. $Zn_{12}O_{12}$, as a novel type of ZnO structure with highest stability in its morphology compared to other structures, has been investigated extensively at the theoretical level [25–33]. Also, the capacity of this nanocluster has been scrutinized for adsorbing various chemicals such as $CO_2$ [34], formic acid, thiophene, NO, and [35]. Sulfur mustard or mustard gas (bis-2-(chloroethyl) sulfide) is known as a substance war agent that is

* Corresponding author.
*E-mail address:* R.rajabzadeh77@gmail.com (H. Rajabzadeh).

https://doi.org/10.1016/j.inoche.2021.109174
Received 30 October 2021; Received in revised form 13 December 2021; Accepted 22 December 2021
Available online 28 December 2021
1387-7003/© 2021 Elsevier B.V. All rights reserved.

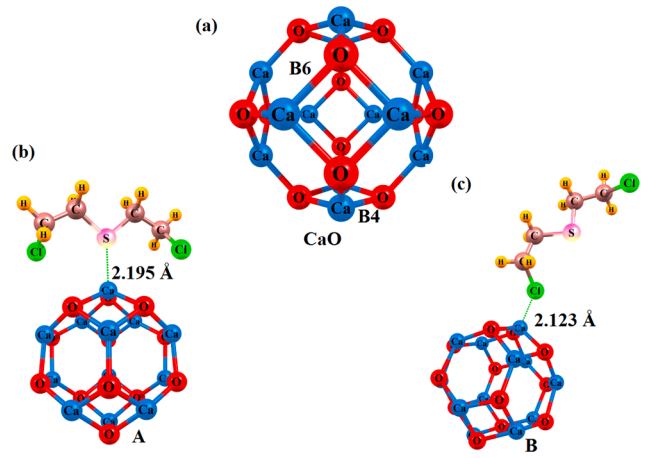


**Fig. 1.** The relaxed structure of (a) $Ca_{12}O_{12}$ nanocluster and (b and c) different complex of CaO/ mustard.

categorized in the armament of mass annihilation [36]. Mustard gas was one of the primary chemical armaments organized in contradiction of troops on a battleground throughout World War I. Later, the military usage of mustard gas has been considered many times [36]. It is very possible that mustard gas can be utilized by terrorists because it is a simple compound voluntarily produced without sumptuous equipment [37]. Furthermore, as a "persistent agent" (US Military organization) aerosolized mustard gas results in a hazard for up to 1 week under dry and warm weather circumstances since it remains in the environment until completely hydrolyzed [38].

Owing to the outstanding characteristics of metal oxide clusters such as $Ca_{12}O_{12}$ nanocluster because of the ionic character and metal-to-oxide bonding, a lot of efforts have been put inro investigating the physical and chemical properties of the clusters mentioned above [39–46]. Using quantum chemistry methods, the $Ca_{12}O_{12}$ nanocluster was recently investigated by Oliveria et al. [47]. They found that this cluster can be used in gas sensors, storage of chemical species, catalysis and adsorption processes [48].

As far as we know, no work has been carried out investigating the adsorption of mustard ($C_4H_8Cl_2S$) molecules onto the external surface of $Ca_{12}O_{12}$ nanoclusters. In this work, we are interested in understanding the impact of the adsorption of mustard molecule upon the electronic and geometric properties of $Ca_{12}O_{12}$ nanoclusters through DFT computations. We analyze the results in light of BEs, NBO charge transfer, MEP, as well as the FMOs.

## 2. Computational details

We carried out the analyses of geometry optimizations, MEP and NBO on a $Ca_{12}O_{12}$ nanocluster and various configurations of $Ca_{12}O_{12}$ nanocluster/ mustard complex at $B_3LYP$-$D_3$ functional and 6-31G* basis set. We also added Grimme's "D" term to this functional. Based on previous studies, the $B_3LYP$-$D_3$ functional is reliable and it is commonly employed to investigate various nanostructures [49–51]. The energy of (AE) related to a mustard molecule on the $Ca_{12}O_{12}$ nanocluster wall is computed as follows:

$$AE = E_{CH_4S/CaO} - E_{CaO} - E_{CH_4S} + E_{BSSE} \quad (1)$$

Here, $E_{mustard/CaO}$ is the total energy of the mustard molecule adsorbed onto the pristine $Ca_{12}O_{12}$ nanocluster. $E_{CaO}$ and $E_{mustard}$ designate, respectively, the energies of the pristine $Ca_{12}O_{12}$ nanocluster and mustard molecule [52]. The energy of the basis set superposition error is designated by $E_{BSSE}$. The negative value of AE refers to an exothermic process, and its positive value refers to an endothermic process. GAMESS software was utilized to perform all of the calculations [53].

## 3. Results and discussion

### 3.1. Optimized geometries of $Ca_{12}O_{12}$ nanocluster and interaction with mustard molecule

$Ca_{12}O_{12}$ nanocluster atomic sites were relaxed at the $B_3LYP$-$D_3$/6-31G*. The $Ca_{12}O_{12}$ nanocluster optimized structure has eight 6-membered (hexagon) rings and six 4-membered (tetragon) rings having tetrahedral symmetry. The side view and the top view of the relaxed structure of this nanocluster are depicted in Fig. 1. As depicted in Fig. 1, there are two Ca-O bonds in this nanocluster, which are not equal in terms of topology. One of these bonds is shared between two hexagon rings ($B_6$), and the other one between the hexagon and tetragon rings ($B_4$). The length of the former is 2.17 Å and that of the latter is 2.21 Å, consistent with the results as maintained de Oliveira et al. [47].

The mustard molecule is situated initially at various sites above the nanocluster with various orientations for finding the most stable adsorption configuration of mustard- $Ca_{12}O_{12}$ nanocluster complex which have the highest stability. In the mustard molecule, the S atom approaches the Ca atom in the nanocluster. in the first orientation, and the Cl atom approaches the Ca atom in the second orientation. Moreover, the S atoms and Cl atoms approach the top center of the tetragon and hexagon rings in other orientations, respectively. Based on the BE values, the adsorption mode with highest stability was chosen for the mustard molecule for further study. Fig. 1 shows the different structures of the mustard molecule which is adsorbed onto the $Ca_{12}O_{12}$ nanocluster surface. According to Fig. 1b, the S atom of mustard is situated near the Ca atoms of the $Ca_{12}O_{12}$ nanocluster tetragon ring. The S-Ca interaction distance is 2.915 Å. The energy of adsorption for the mustard molecule on the $Ca_{12}O_{12}$ nanocluster (complex A) is −46.07 kJ/mol, which shows the physical adsorption of the mustard molecule onto the nanocluster. Based on the adsorption energy, this complex is weakly adsorbed onto the $Ca_{12}O_{12}$ nanocluster. Finally, in complex B, as shown in Fig. 1c, the Cl atom of mustard is close to Ca atoms of $Ca_{12}O_{12}$ nanocluster. The distance from the Cl atom to the Ca atom is approximately 2.123 Å. The adsorption of the mustard molecule onto the nanocluster surface is exothermic to a great extent (i.e., −129.18 kJ/mol). The greater BE of complex B in comparison to other complexes might be because of the shorter interaction distance between Cl and in complex (B) in contrast to interaction between the S atoms and the Ca atoms. In other words, the higher electronegativity of the Cl atom than the sulfur atom has caused this phenomenon.

### 3.2. Charge transport and MEP analysis

As shown in Table 1, the net charge transport on molecules was

**Table 1**
Calculated adsorption energy (AE/kJ/mol), HOMO energies ($E_{HOMO}$/eV), LUMO energies ($E_{LUMO}$/eV), HOMO-LUMO energy gap ($E_g$/eV), and Fermi level energy ($E_F$/eV), for all the systems.

| Structure | AE | HOMO | LUMO | $E_{g\text{-}gas}$ | $E_F$ | $\Delta E_g$ (%) | $E_{g\text{-}solv}$ |
|---|---|---|---|---|---|---|---|
| $Ca_{12}O_{12}$ nanocluster | – | −5.56 | −0.89 | 4.67 | −3.23 | – | 4.69 |
| Complex A | −46.07 | −4.14 | −0.78 | 3.36 | −2.46 | 28.16 | – |
| Complex B | −129.18 | −3.08 | −0.69 | 2.38 | −1.89 | 48.96 | 2.58 |

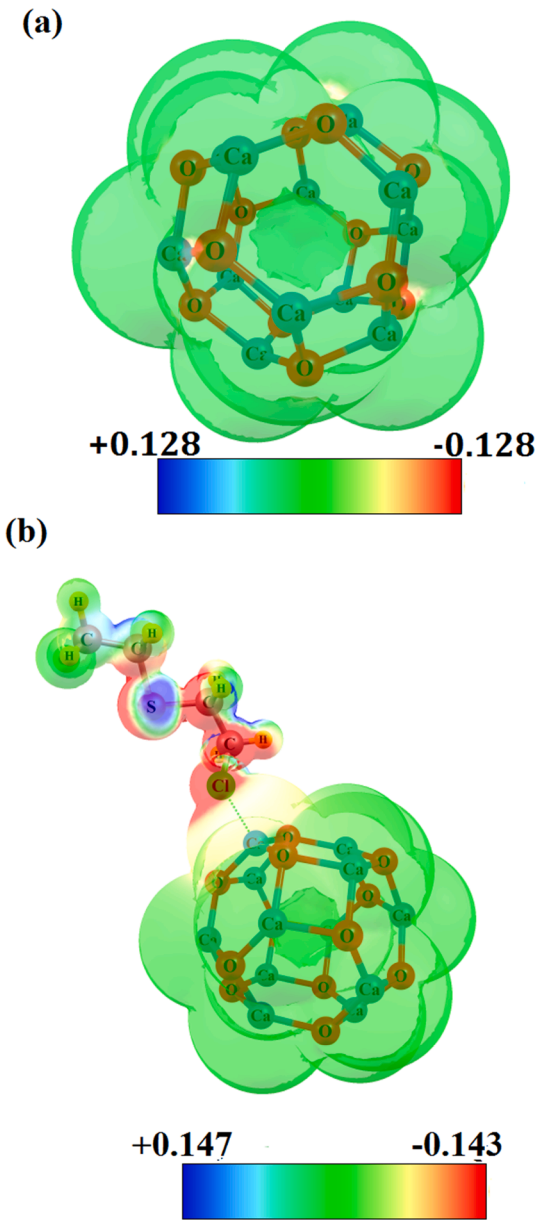


**Fig. 2.** Molecular electrostatic potential of (a) pristine $Ca_{12}O_{12}$ nanocluster, (b) Complex B of $Ca_{12}O_{12}$ nanocluster /mustard.

computed through NBO to predict the influence of the adsorption of mustard molecule over the electronic characteristics of the $Ca_{12}O_{12}$ nanocluster. The NBO charge transport to the mustard molecule from the nanocluster (complex B) is 0.437 e, which is consistent with the high BE as well as the short binding distances in complex B. Based on our findings, binding energy bears a direct relationship to charge transfer. In complex B, the binding distance is higher compared to other complexes, which leads to higher BE and transport of charge. The Ca atoms in this nanocluster have negative charge (+1.478 e/atom) whereas the O atoms are rich in electron (−1.478 e/atom). In the interaction area, the charge of Ca atoms reduced to +1.429 and that of the O atoms reduced to −1.609 e. As shown in Fig. 2, we can further explore the effects of mustard adsorption over the nanocluster electronic structure using an MEP map. Due to the symmetrical structure of free $Ca_{12}O_{12}$ nanocluster, as shown in Fig. 2a, it possesses symmetrical potential. O atoms possess negative potential whereas Ca atoms possess positive potential. The positive charges in $Ca_{12}O_{12}$ nanocluster are strengthened following the adsorption of mustard molecules on the surface of this nanocluster,

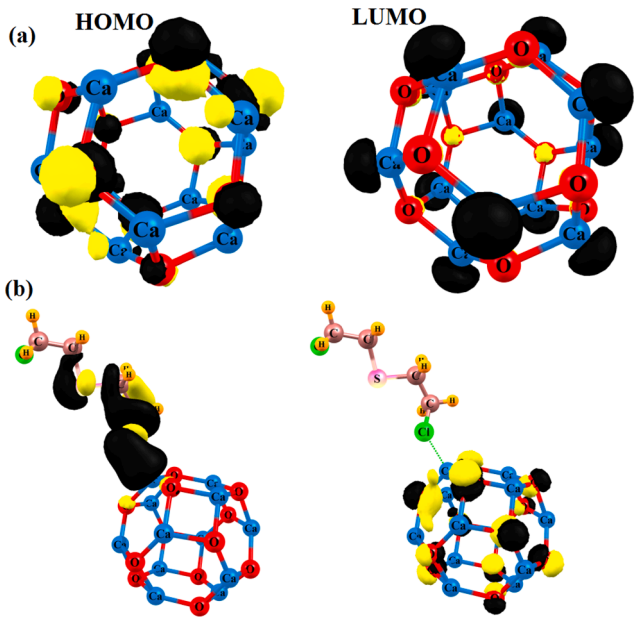


**Fig. 3.** HOMO-LUMO distributions of (a) pristine $Ca_{12}O_{12}$ nanocluster, (b) Complex B of $Ca_{12}O_{12}$ nanocluster /mustard.

which is in agreement with the transport of negative charge on mustard molecules, leaving a positive charge on $Ca_{12}O_{12}$ nanocluster.

### 3.3. Analysis of FMOs

We investigated the FMOs of the free $Ca_{12}O_{12}$ nanocluster and complex C in order to further understand the influence of the mustard molecule adsorption over the electronic characteristics of the nanocluster. Fig. 3 depicts the HOMO and LUMO distributions and Table 1 lists the HOMO-LUMO energy band gap ($E_g$), the HOMO and LUMO energies, and the Fermi level energy ($E_{FL}$). At T = 0 K, $E_{FL}$ is situated almost in the middle of the HOMO-LUMO energy gap. Based on $E_g$ of HOMO-LUMO of this nanocluster which is 4.67 eV, it can be said this nanocluster is a semiconductor, and this value is consistent with the values reported in the literature. Based on the literature, $Ca_{12}O_{12}$ nanocluster is a a semiconductor with a wide band gap (4.00 eV) [47]. The HOMO is mainly located on O atoms, but the LUMO density on the nanocluster is very small. major changes occur in the FMOs following the interaction of the mustard molecule (complex B) with the nanocluster. The localization of the HOMO is localized more on the mustard molecule in contrast with the LUMO that does not change, which shows that the LUMO is a contributory factor in the dissociation process (Fig. 3). The changes in the HOMO density are significant, but the LUMO density of the complex is similar to the LUMO density of the free nanocage. It is worth mentioning that the change in the band gap results in the changes in conductivity, which is a contributory factor in designing sensors. The relationship between $E_g$ and conductivity can be described by the equation below [54]:

$$\sigma \propto exp\left(\frac{-E_g}{kT}\right) \tag{2}$$

where k designates the Boltzmann constant and σ designates the electric conductivity. It goes without saying that when the band gap is reduced to a small extent, the electrical conductivity is dramatically increased. The $Ca_{12}O_{12}$ nanocluster band gap decreased by 2.29 eV (48.93%) following its interaction with mustard molecules. We can, therefore, conclude that $Ca_{12}O_{12}$ nanocluster can be employed as a sensor for the adsorption of the mustard molecule.

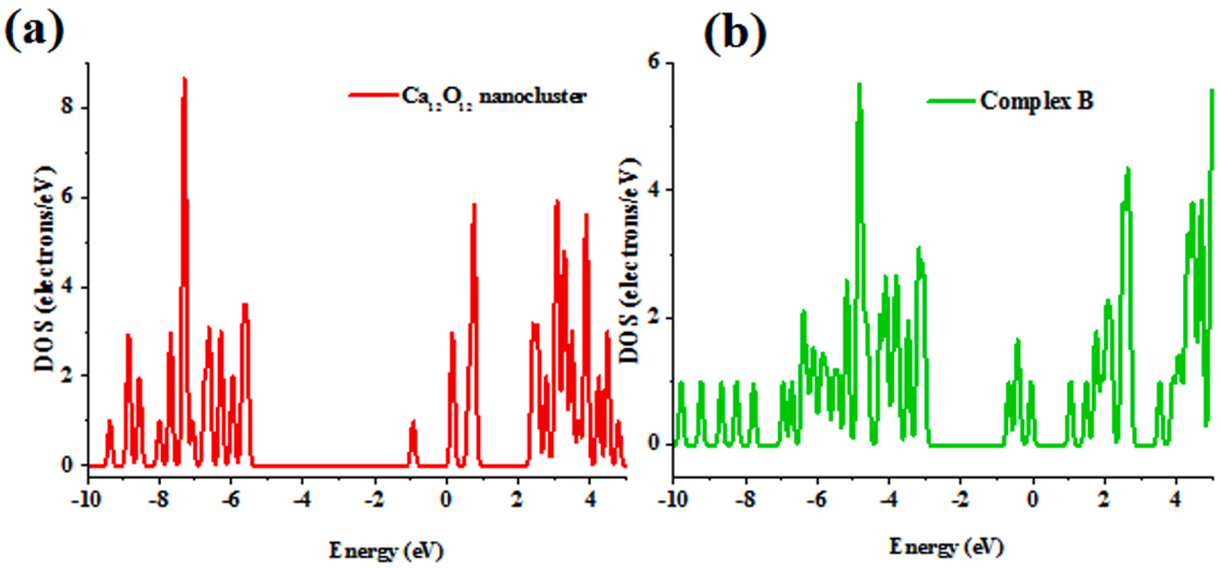


**Fig. 4.** DOS plot of (a) pristine $Ca_{12}O_{12}$ nanocluster, (b) Complex B of $Ca_{12}O_{12}$ nanocluster /mustard.

### 3.4. Density of states analysis

The changes in the electronic states are revealed from the changes in the density of states (DOS) during the adsorption process. The DOS for the configurations B of mustard adsorption on the $Ca_{12}O_{12}$ nanocluster and pristine $Ca_{12}O_{12}$ nanocluster are shown in Fig. 4. Earlier, the $Ca_{12}O_{12}$ nanocluster shows an energy gap of 4.67 eV. Based on the interaction of the mustard gas with nanocluster the DOS spectrum of the $Ca_{12}O_{12}$ nanocluster was changed and also decreases the band gap of $Ca_{12}O_{12}$ nanocluster. The reason DOS plot changes after gas adsorption with related to the below: it is well known that the molecule such as mustard gas owing to the unique structure, the band gap decreases compared to the isolated $Ca_{12}O_{12}$ nanocluster. It infers that the charge transfer takes place. Besides, the change in the peaks along the valence and conduction band is noticed for complex mustard/$Ca_{12}O_{12}$ nanocluster. Thus, the DOS spectrum and band structure reveals that the adsorption of mustard gas results in the electron transmission between mustard gas molecules and $Ca_{12}O_{12}$ nanocluster material that is noticed from the peak shift and variation in the DOS spectrum on various energy levels.

### 3.5. Analysis of recovery time

The recovery of sensors from adsorbed gasses is important. Based on experiments, we can heat adsorbents to higher temperatures or expose them to Ultraviolet (UV) light to evaluate recovery time (τ) [55]. We can compute τ from transition theory as follows:

$$\tau = \frac{1}{\nu}\left[exp\left(\frac{-AE}{kT}\right)\right] \quad (3)$$

where υ is the attempt frequency, T designates the temperature and k designates the Boltzmann constant (~$8.31 \times 10^{-3}$ kJ $mol^{-1}$.K). In case an attempt frequency of approximately 1012 $s^{-1}$ is applied (used for the recovery of carbon nanotubes at ambient temperature [56]), τ of mustard molecules in complex C will be approximately 93.85 ms, which shows the short recovery time of the $Ca_{12}O_{12}$ nanocluster as a sensor.

### 3.6. The impact of solvent

The PMC method was employed to scrutinize the impact of the change in the solvent upon the adsorption mustard gas onto the nanocluster. In the aqueous phase, the solvent had insignificant impact upon the electronic and structural characteristics of the nanocluster. However, the solvent impact upon the geometric parameters of complex B is significant. In contrast with AE values for adsorptions in the gas phase, the related AE values in the aqueous phase are less negative based on Table 1. Based on the results, the interaction between the mustard gas and the $Ca_{12}O_{12}$ nanocluster in the aqueous phase is weaker compared to the interaction in the gas phase. In our opinion, an increase in the stabilization of the mustard molecule which is due to the solvent leads to an increase in reactivity. The $E_g$ value of complex B in the aqueous phase is higher compared to that of the gas phase by approximately 0.193 eV. Nonetheless, the solvent impact upon on the electronic characteristics of the above-mentioned complexes does not significantly affect the sensor signal.

## 4. Conclusions

The adsorption of mustard molecule was scrutinized onto the $Ca_{12}O_{12}$ nanocluster through DFT computations. Based on this method, the adsorption geometry, BE, NBO charge transport, MEP, frontier molecular orbitals, as well as PCM effect of activities of pure $Ca_{12}O_{12}$ nanocluster with the adsorption of mustard molecule were investigated. It was found that this nanocluster can be employed as a promising sensor for detecting mustard gas since the charge transfer is large and there is a reduction in $E_g$ of this nanocluster. Also, the decrease in the energy band gap in the mustard/ $Ca_{12}O_{12}$ nanocluster complex was found to be mainly because of the HOMO destabilization. Nevertheless, there is almost no change in the LUMO energy level. The impact of the solvent upon the electronic characteristics and the geometry parameters of the mustard/ $Ca_{12}O_{12}$ nanocluster complexes is significant. In addition, in the aqueous phase, the interaction among components is weaker to a great extent compared to the interaction in vacuum. Moreover, the recovery time of the mustard molecules in complex C was calculated to be 93.85 ms. Based on the theoretical findings in this work, we can use the $Ca_{12}O_{12}$ nanocluster as a sensitive sensor to detect the mustard molecule.

## Declaration of Competing Interest

The authors declare that they have no known competing financial interests or personal relationships that could have appeared to influence the work reported in this paper.

## References


[1] H.W. Kroto, J.R. Heath, S.C. O'Brien, R.F. Curl, R.E. Smalley, C 60: buckminsterfullerene, Nature 318 (1985) 162–163.
[2] S.-H. Xu, M.-Y. Zhang, Y.-Y. Zhao, B.-G. Chen, J. Zhang, C.-C. Sun, Stability and property of planar (BN) x clusters, Chem. Phys. Lett. 423 (2006) 212–214.
[3] A. Davoodnia, Z.-B. Atefeh, H. Behmadi, A rapid and green method for solvent-free synthesis of 1, 8-dioxodecahydroacridines using tetrabutylammonium hexatungstate as a reusable heterogeneous catalyst, Chin. J. Catal. 33 (2012) 1797–1801.
[4] T. Dudo, M.M. Turnbull, J.L. Wikaira, SYNTHESIS, CRYSTAL STRUCTURE AND MAGNETIC PROPERTIES OF BIS (3-AMINO-2-CHLOROPYRIDINE) DIBROMIDOCOPPER (II), EUROPEAN CHEMICAL BULLETIN 9 (2020) 174–178.
[5] O.V. Mikhailov, D.V. Chachkov, Molecular structure models of Al2Ti3 and Al2V3 clusters according to DFT quantum-chemical calculations, Eur. Chem. Bull. 9 (2020) 62–68.
[6] Z. Duan, C. Li, W. Duan, Y. Zhang, M. Yang, T. Gao, et al., Milling force model for aviation aluminum alloy: academic insight and perspective analysis, Chin. J. Mech. Eng. 34 (2021) 1, https://doi.org/10.1186/s10033-021-00536-9.
[7] S.M. Ismail, Cholinesterase and Aliesterase as a Natural Enzymatic Defense against Chlorpyrifos in Field Populations of Spodoptera Littoralis (Boisdüval, 1833) (Lepidoptera, Noctüidae), J. Plant Bioinform. Biotechnol. 1 (2021) 41–50.
[8] A.A. Al-Kahtani, S. Tabassum, I. Raya, I.H. Khlewee, S. Chupradit, A. Davarpanah, et al., Influence of different rotations of organic formamidinium molecule on electronic and optical properties of FAPbBr 3 Perovskite, Coatings. 11 (2021) 1341.
[9] M. Liu, C. Li, C. Cao, L. Wang, X. Li, J. Che, Walnut fruit processing equipment: academic insights and perspectives, Food Eng. Rev. 13 (2021) 822–857.
[10] S.S. Gadekar, S.B. Sapkal, B.R. Madje, HEPES BUFFER MEDIATED SYNTHESIS OF 3, 4-DIHYDRO-3, 3-DIMETHYL-9-ARYLACRIDIN-1-ONES, EUROPEAN CHEMICAL BULLETIN 9 (2020) 6–9.
[11] P.G. Pathare, S.U. Tekale, M.G. Damale, J.N. Sangshetti, R.U. Shaikh, L. Kótai, et al., PYRIDINE AND BENZOISOTHIAZOLE BASED PYRAZOLINES: SYNTHESIS, CHARACTERIZATION, BIOLOGICAL ACTIVITY, MOLECULAR DOCKING AND ADMET STUDY, EUROPEAN CHEMICAL BULLETIN 9 (2020) 10–21.
[12] T.G. Giorgadze, I.G. Khutsishvili, Z.G. Melikishvili, V.G. Bregadze, SILVER ATOMS ENCAPSULATED IN G4 PAMAM (POLYAMIDOAMINE) DENDRIMERS AS A MODEL FOR THEIR USE IN NANOMEDICINE FOR PHOTOTHERAPY, EUROPEAN CHEMICAL BULLETIN. 9 (2020) 22–27.
[13] Y. Wang, C. Li, Y. Zhang, M. Yang, B.K. Li, L. Dong, et al., Processing characteristics of vegetable oil-based nanofluid MQL for grinding different workpiece materials, Int. J. Precis. Eng. Manuf. - Green Technol. 5 (2018) 327–339.
[14] D.V. Chachkov, O.V. Mikhailov, Novel modifications of elemental nitrogen and their molecular structures–a quantum-chemical calculation, Eur. Chem. Bull. 9 (2020) 78–81.
[15] L.N. Okoro, G. Joel, Advanced nanocatalysts for biodiesel production, Eur. Chem. Bull. 9 (2020) 148–153.
[16] J. Sonar, S. Pardeshi, S. Dokhe, K. Kharat, A. Zine, L. Kótai, et al., Synthesis and anti-proliferative screening of newthiazole compounds, Eur. Chem. Bull. 9 (2020) 132–137.
[17] D.R. Birhade, R.G. Shinde, M.N. Lokhande, M.D. Nikalje, Synthesis of (±)-Baclofen using Wittig Olefination-Claisen Rearrangement, J. Appl. Organometallic Chem. 1 (2021) 109–115.
[18] S. Chupradit, A.T. Jalil, Y. Enina, D.A. Neganov, M.S. Alhassan, S. Aravindhan, A. Davarpanah, A. Ahmed, Use of organic and copper-based nanoparticles on the turbulator installment in a shell tube heat exchanger: a CFD-Based simulation approach by using nanofluids, J. Nanomater. 2021 (2021) 1–7.
[19] J. Beheshtian, A.A. Peyghan, Z. Bagheri, M. Kamfiroozi, Interaction of small molecules (NO, H 2, N 2, and CH 4) with BN nanocluster surface, Struct. Chem. 23 (2012) 1567–1572.
[20] J. Beheshtian, M. Kamfiroozi, Z. Bagheri, A.A. Peyghan, B12N12 nano-cage as potential sensor for NO2 detection, Chin. J. Chem. Phys. 25 (2012) 60.
[21] J. Beheshtian, Z. Bagheri, M. Kamfiroozi, A. Ahmadi, Toxic CO detection by B12N12 nanocluster, Microelectron. J. 42 (2011) 1400–1403.
[22] J. Beheshtian, A.A. Peyghan, Z. Bagheri, Arsenic interactions with a fullerene-like BN cage in the vacuum and aqueous phase, J. Mol. Model. 19 (2013) 833–837.
[23] S. Giri, A. Chakraborty, P. Chattaraj, Stability and aromaticity of nH2@ B12N12 (n= 1–12) clusters, Nano Rev. 2 (2011) 5767.
[24] J. Antony, X. Chen, J. Morrison, L. Bergman, Y. Qiang, D.E. McCready, et al., ZnO nanoclusters: synthesis and photoluminescence, Appl. Phys. Lett. 87 (2005) 241917.
[25] C. Couillaud, R. Deicas, P. Nardin, M. Beuve, J. Guihaumé, M. Renaud, et al., Ionization and stopping of heavy ions in dense laser-ablated plasmas, Phys. Rev. E 49 (1994) 1545.
[26] J.M. Matxain, J.M. Mercero, J.E. Fowler, J.M. Ugalde, Electronic excitation energies of Zn i O i clusters, J. Am. Chem. Soc. 125 (2003) 9494–9499.
[27] A. Reber, S. Khanna, J. Hunjan, M. Beltran, Rings, towers, cages of ZnO, Eur. Phys. J. D 43 (2007) 221–224.
[28] M. Yoosefian, Powerful greenhouse gas nitrous oxide adsorption onto intrinsic and Pd doped Single walled carbon nanotube, Appl. Surf. Sci. 392 (2017) 225–230.
[29] X.-Y. Li, Y. Song, C.-X. Zhang, C.-X. Zhao, C. He, Inverse CO2/C2H2 separation in a pillared-layer framework featuring a chlorine-modified channel by quadrupole-moment sieving, Sep. Purif. Technol. 279 (2021) 119608.
[30] T. Wang, W. Liu, J. Zhao, X. Guo, V. Terzija, A rough set-based bio-inspired fault diagnosis method for electrical substations, Int. J. Electr. Power Energy Syst. 119 (2020) 105961.
[31] J. Sun, H. Du, Z. Chen, L. Wang, G. Shen, MXene quantum dot within natural 3D watermelon peel matrix for biocompatible flexible sensing platform, Nano Res. 1–7 (2021).
[32] X. Zhang, Y. Tang, F. Zhang, C.S. Lee, A novel aluminum–graphite dual-ion battery, Adv. Energy Mater. 6 (2016) 1502588.
[33] B. Jamalvandi, Z. Arzehgar, J. Med. Chem. Sci. (2021).
[34] J. Qaderi, A brief review on the reaction mechanisms of CO2 hydrogenation into methanol, Int. J.Innovative Res. Sci. Stud. 3 (2020) 53–63.
[35] R. Razavi, S.M. Abrishamifar, H.A. Toupkanloo, M.J. Lariche, M. Najafi, DFT investigation of the potential of B 21 N 21 and Al 21 P 21 nanocages as anode electrodes in metal ion batteries, J. Cluster Sci. 29 (2018) 879–887.
[36] V. Paromov, Z. Suntres, M. Smith, W.L. Stone, Sulfur mustard toxicity following dermal exposure: role of oxidative stress, and antioxidant therapy, J. Burns Wounds (2007) 7.
[37] B. Li, C. Li, Y. Zhang, Y. Wang, D. Jia, M. Yang, N. Zhang, Z. Han, K. Sun, Heat transfer performance of MQL grinding with different nanofluids for Ni-based alloys using vegetable oil, J. Clean. Prod. 154 (2017) 1–11, https://doi.org/10.1016/j.jclepro.2017.03.213.
[38] G. Prasad, T. Mahato, B. Singh, P. Pandey, A. Rao, K. Ganesan, et al., Decontamination of sulfur mustard on manganese oxide nanostructures, AIChE J. 53 (2007) 1562–1567.
[39] L. Chen, G.-Q. Zhou, C. Xu, T. Zhou, Y. Huo, Structural and electronic properties of hydrated MgO nanotube clusters, J. Mol. Struct. (Thoechem) 900 (2009) 33–36.
[40] M. Haertelt, A. Fielicke, G. Meijer, K. Kwapien, M. Sierka, J. Sauer, Structure determination of neutral MgO clusters—hexagonal nanotubes and cages, PCCP 14 (2012) 2849–2856.
[41] K. Kwapien, M. Sierka, J. Döbler, J. Sauer, M. Haertelt, A. Fielicke, et al., Structural Diversity and Flexibility of MgO Gas-Phase Clusters, Angew. Chem. Int. Ed. 50 (2011) 1716–1719.
[42] M. Yoosefian, N. Etminan, A. Juan, E. Mirhaji, Ultra-low concentration protein detection based on phenylalanine–Pd/SWCNT as a high sensitivity nanoreceptor, RSC Adv. 10 (2020) 2650–2660.
[43] M. Yoosefian, A. Pakpour, N. Etminan, Nanofilter platform based on functionalized carbon nanotubes for adsorption and elimination of Acrolein, a toxicant in cigarette smoke, Appl. Surf. Sci. 444 (2018) 598–603.
[44] M. Yoosefian, N. Etminan, Leucine/Pd-loaded (5, 5) single-walled carbon nanotube matrix as a novel nanobiosensors for in silico detection of protein, Amino Acids 50 (2018) 653–661.
[45] M. Yoosefian, A high efficient nanostructured filter based on functionalized carbon nanotube to reduce the tobacco-specific nitrosamines, NNK. Applied Surface Science. 434 (2018) 134–141.
[46] F.A. Zaghmarzi, M. Zahedi, A. Mola, S. Abedini, S. Arshadi, S. Ahmadzadeh, et al., Fullerene-C60 and crown ether doped on C60 sensors for high sensitive detection of alkali and alkaline earth cations, Physica E 87 (2017) 51–58.
[47] O.V. de Oliveira, J.M. Pires, A.C. Neto, J.D. dos Santos, Computational studies of the Ca12O12, Ti12O12, Fe12O12 and Zn12O12 nanocage clusters, Chem. Phys. Lett. 634 (2015) 25–28.
[48] S. Guo, C. Li, Y. Zhang, Y. Wang, B. Li, M. Yang, X. Zhang, G. Liu, Experimental evaluation of the lubrication performance of mixtures of castor oil with other vegetable oils in MQL grinding of nickel-based alloy, J. Clean. Prod. 140 (2017) 1060–1076, https://doi.org/10.1016/j.jclepro.2016.10.073.
[49] A.A. Peyghan, H. Soleymanabadi, Adsorption of H2S at Stone-Wales defects of graphene-like BC3: a computational study, Mol. Phys. 112 (2014) 2737–2745.
[50] A. Soltani, A.A. Peyghan, Z. Bagheri, H2O2 adsorption on the BN and SiC nanotubes: a DFT study, Physica E 48 (2013) 176–180.
[51] A.A. Peyghan, H. Soleymanabadi, Computational study on ammonia adsorption on the X 12 Y 12 nano-clusters (X = B, Al and Y = N, P), Curr. Sci. 1910–4 (2015).
[52] Y. Wang, C. Li, Y. Zhang, B. Li, M. Yang, X. Zhang, S. Guo, G. Liu, Experimental evaluation of the lubrication properties of the wheel/workpiece interface in MQL grinding with different nanofluids, Tribol. Int. 99 (2016) 198–210, https://doi.org/10.1016/j.triboint.2016.03.023.
[53] A.L. Tenderholt, K.M. Langner, N.M. O'Boyle, A library for package-independent computational chemistry algorithms, J. Comp. Chem (2008) 839–845.
[54] N.L. Hadipour, A. Ahmadi Peyghan, H. Soleymanabadi, Theoretical study on the Al-doped ZnO nanoclusters for CO chemical sensors, J. Phys. Chem. C 119 (2015) 6398–6404.
[55] J. Li, Y. Lu, Q. Ye, M. Cinke, J. Han, M. Meyyappan, Carbon nanotube sensors for gas and organic vapor detection, Nano Lett. 3 (2003) 929–933.
[56] S. Peng, K. Cho, P. Qi, H. Dai, Ab initio study of CNT NO2 gas sensor, Chem. Phys. Lett. 387 (2004) 271–276.